Supplementary Materials for

Electrocaloric cooling with latent heat transfer enabling high power density

Authors: Julius Metzdorf[1], Patrick Corhan[1], David Bach[1], Sakyo Hirose[2], Dirk Lellinger[3], Stefan Mönch[4], Frank Kühnemann[1], Olaf Schäfer-Welsen[1], Kilian Bartholomé[1*]

Affiliations:

[1]Fraunhofer Institute for Physical Measurement Techniques IPM; Freiburg, 79110, Germany.

[2]Murata Manufacturing Co., Ltd., 1-10-1, Higashikotari, Nagaokakyo; Kyoto 617-8555, Japan.

[3]Fraunhofer Institute for Structural Durability and System Reliability LBF; 64289 Darmstadt, Germany.

[4]Fraunhofer Institute for Applied Solid State Physics IAF; Freiburg, 79108, Germany.

*Corresponding author. Email: Kilian.Bartholome@ipm.fraunhofer.de

The PDF file includes:

Other Supplementary Materials for this manuscript include the following:

Supplementary Text: Thermal stabilization of EC-components

The AEH system needs a thermal stabilization mechanism, otherwise the temperature of the EC-components is slowly increasing, which leads to a failure of the heat transfer mechanism. There are three reasons, why a thermal stabilization is needed.

1. Thermodynamic cycle
2. Hysteresis of EC-material
3. Temperature dependence of enthalpy the of evaporation

This is explained now in more detail by considering the steps of an EC-cycle. It is important to have in mind, that in a heat pipe the relevant heat transfer mechanism is condensation and evaporation of fluid. The amount of heat $\dot{Q}$ transferred by this process is proportional to the mass flow $\dot{m}$ and the enthalpy of evaporation Δh_V:

$$\dot{Q} = \dot{m}\, \Delta h_V \tag{1}$$

The enthalpy of evaporation is temperature dependent $\Delta h_V = \Delta h_V(T) = \Delta h_V^T$ and is monotonically decreasing with rising temperature. The hotter a liquid is, the less energy is needed to evaporate it: $\Delta h_V^{T_h} < \Delta h_V^{T_C}$.

Let us think of a Carnot cycle in a Temperature-entropy diagram, like shown in fig. S1.

Now we consider the steps of a cooling cycle:

1. Field is turned off, the EC-components cool down and absorb heat from the condensing fluid:

$$Q_c = m_c\, \Delta h_V^{T_C} \tag{2}$$

2. Field is turned on, the work $W = \Delta s\, \Delta T$ is done to drive the EC-effect and the components heat up. This is shown in fig. S1. with the green dashed line. Real capacitors also show hysteresis. For simplicity it is assumed that the whole dissipative losses due to hysteresis occur while turning the field on. Then the heat in the heating part of the cycle is greater than the absorbed heat in the cooling part.

$$Q_h = Q_c + W + Q_{diss} > Q_k \tag{3}$$

So, to expel all heat, a liquid fluid mass of

$$m_h = \Delta h_V^{T_h}\, Q_h = \Delta h_V^{T_h}(Q_c + W + Q_{diss}) > m_c \tag{4}$$

is necessary.

As only m_c is in liquid form on the surface of the EC-components, the additional heat remains in the EC-components and heats up the EC-components (under sufficiently adiabatic conditions). So, after one full cycle the EC-components are slightly warmer than before. The effect of hysteresis on the EC-performance is discussed in more detail in [23].

3. If now the field is turned off again, the EC-components cool down but a bit less than in the cycle before, because the extra heat from the last cycle is absorbed first. A bit less of the reversible EC-effect can be used to cool down the EC-components, which in turn, leads to a bit less condensed fluid. Less condensing fluid means less transferred heat.

Finally, after several cycles, no fluid condenses on the warmed-up EC-components and no heat can be transferred anymore.

Local fluid return: Concept and Implementation

The concept of the local fluid return is to transport some extra liquid fluid m_{FR} on the surface of the EC-components, so that the extra heat from the dissipative losses can be transferred to the fluid. Like this the EC-components are thermally stabilized and all heat during the heating can be expelled:

$$Q_h = m_h \, \Delta h_V = \Delta h_V (m_c + m_{FR}) \tag{5}$$

The local fluid return transports some extra fluid to the segment to balance the mass and heat flows, like schematically shown in fig. S2 and fig. S3.

The EC-components have a hydrophilic surface coating, which improves the wetting properties. For a homogenous thermal stabilization, the local fluid return is attached to both sides of the components (see fig S5).

Experimental proof of principle for local fluid return

In fig. S4 the temporal evolution of a segment without thermal stabilization is compared to a segment thermally stabilized by a local fluid return.

In a system without thermal stabilization, to build up a temperature difference, the electric field strength was raised slowly over several minutes, so that the EC-components could fully exchange heat with the environment (see inset of fig. S4).
Then the field was turned off, the EC-components cooled down below the temperature of the evaporator and fluid condensed on the EC-components. Now a sinusoidal field was applied to run the electrocaloric cooling cycle. At the beginning of cycling the condensed liquid is sufficient to transfer the heat from the EC-components. As dissipative losses slowly heat up the EC-components, each cycle a little bit more fluid evaporates than condenses. This leads to a dry-out of the EC-components and an interruption of heat transfer, which leads to a breakdown of the established temperature difference. The performance of the segment with thermal stabilization is stable over time. More time is needed to establish a temperature difference. This is because more liquid fluid and thereby more thermal mass is present in the segment. The aspect, that the system with thermal stabilization leads to slightly smaller temperature spans can be explained by the additional fluid in the segment which corresponds to a larger thermal mass.

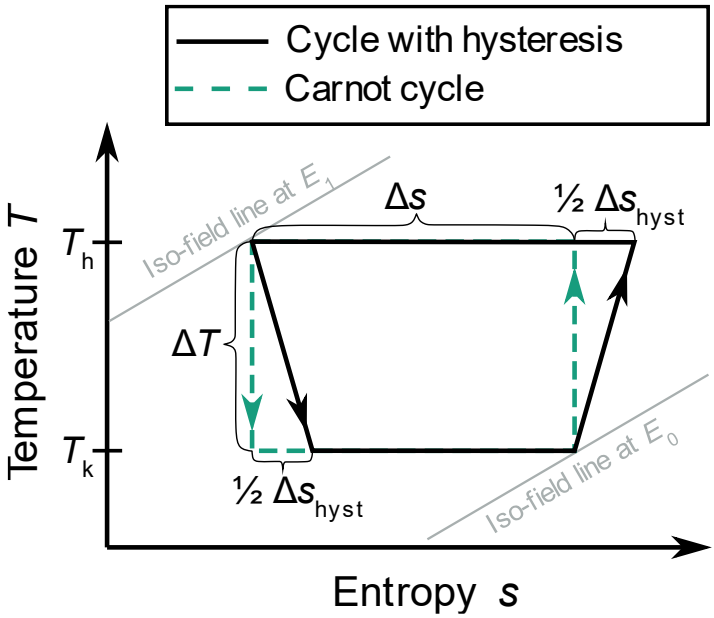

Fig. S1.

A Carnot cycle (green dashed line) in the temperature – entropy diagram for an electrocaloric material between zero field E_0 and applied field E_1. The solid black line shows a cycle with hysteresis. Illustration adapted from Hess et al.[23]

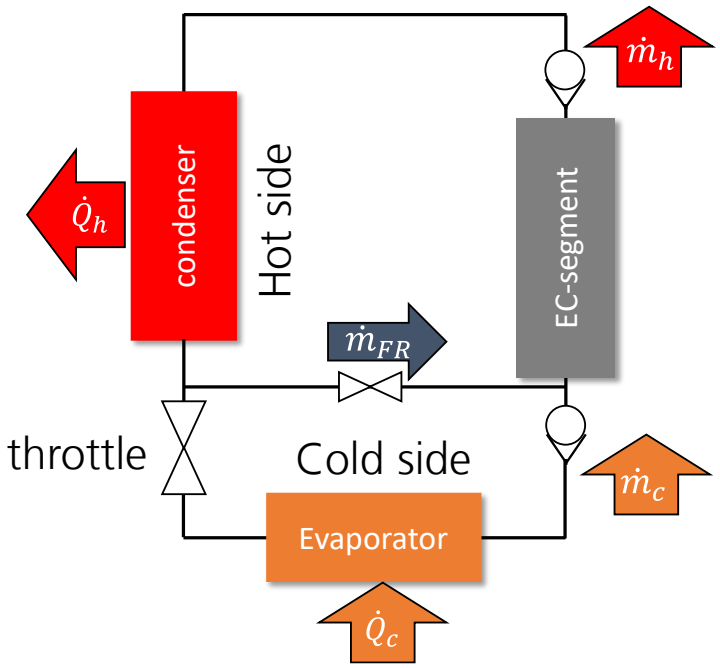

Fig. S2.

The heat and mass flows of the AEH. The wick transports the fluid from the condenser to the evaporator, like a throttle in a vapor-compression cycle. Some of the fluid mass is transported via the local fluid return (FR) directly to the segment to balance the mass flows and thermally stabilize the EC-components.

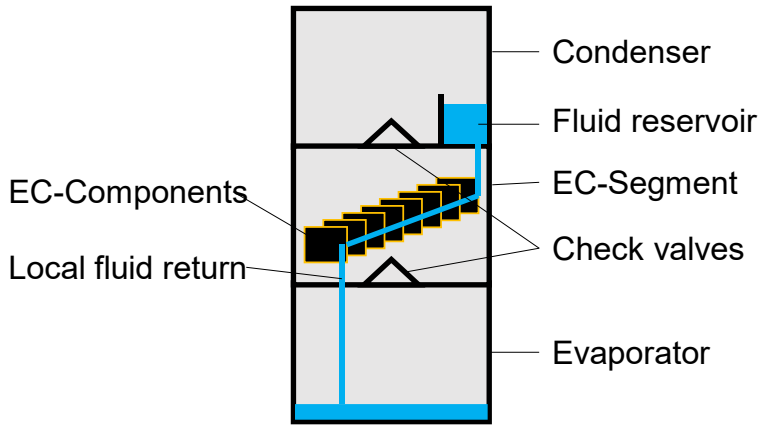

Fig. S3.

Simple illustration of the setup with local fluid return. If an alternating field is applied to the EC-components, heat and fluid is transported from the evaporator through the EC-segment to the condenser. The fluid reservoir feeds the local fluid return, which stabilizes the EC-components.

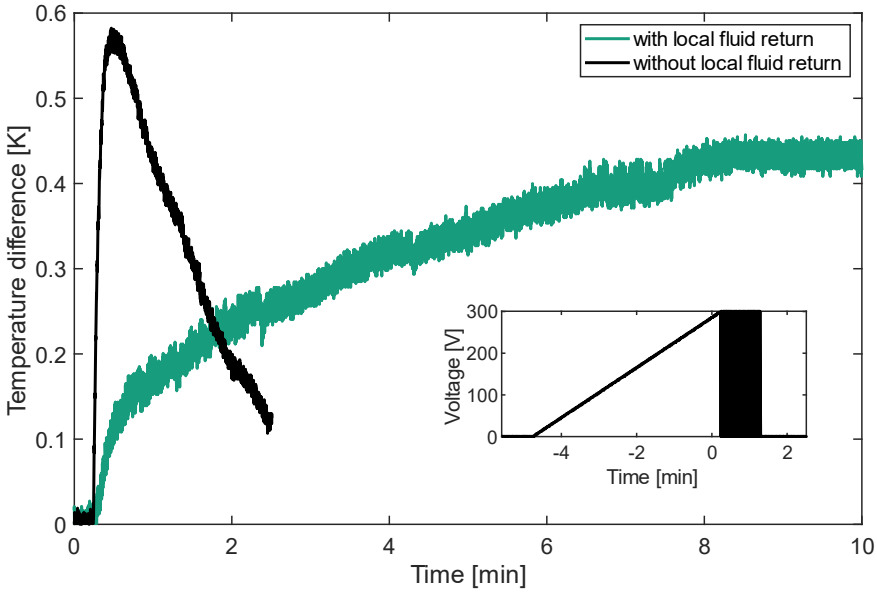

Fig. S4.

Temporal evolution of temperature difference of a segment without thermal stabilization (black line) and a segment with thermal stabilization (green line) provided by a local fluid return. To establish a temperature difference without local fluid return, the voltage was increased slowly over 5 min, so that the EC-components could fully thermalize with the environment (see inset). Then the voltage is removed, so that liquid condenses on the EC-components. Then a sinusoidal voltage is applied and a temperature difference can be established for a short time. Then the EC-components heat up and the temperature difference decreases despite the applied voltage. After roughly 2.5 min the measurement was stopped. The green curve is the temperature difference established by a segment with local fluid return. More time is needed to establish a temperature difference, because more fluid and thus more thermal mass is present in the segment. The segment with local fluid return reaches a steady state.

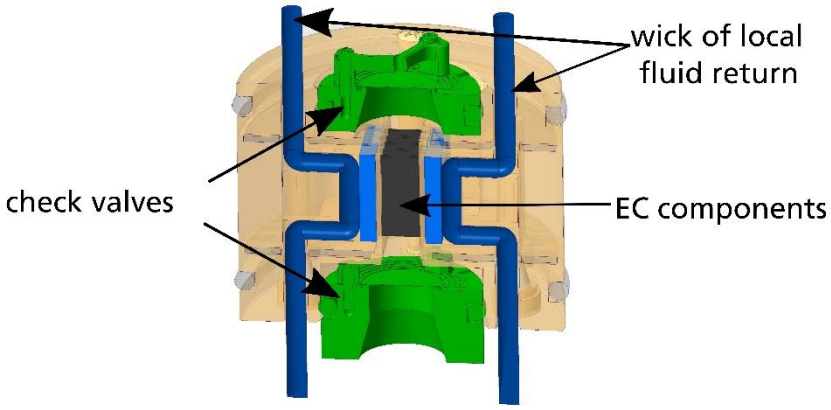

Fig. S5.

Schematic cross-section of the segment. The check valves (green), the EC components (dark grey) and the local fluid return (blue) are highlighted.

For a homogenous thermal stabilization, the local fluid return is attached to both sides of the components.

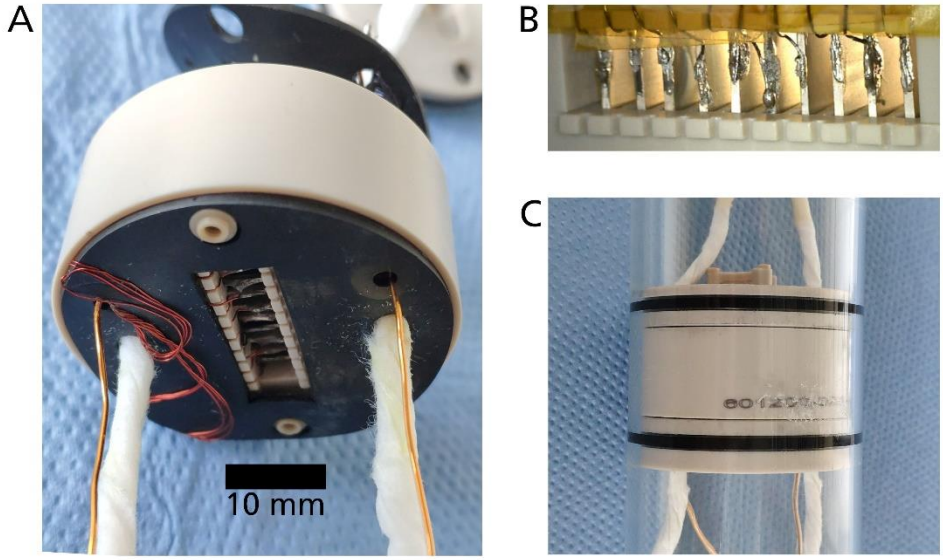

Fig. S6.

Experimental realization of the segment. (A) shows the half-open segment. PST components are in the middle, each electrically contacted with a thin wire with red protective coating. The thin wires are soldered to the thicker left copper wire. The right copper wire is connected to the other side of the PST components. The wick of the local fluid return (white) can be seen on both sides. (B) shows the PST MLCs components, which are placed in slits in the housing made of Polyether ether ketone (PEEK). (C) shows the finished segment within the glass tube as it is used in the setup. On the upper side part of the check valve can be seen.

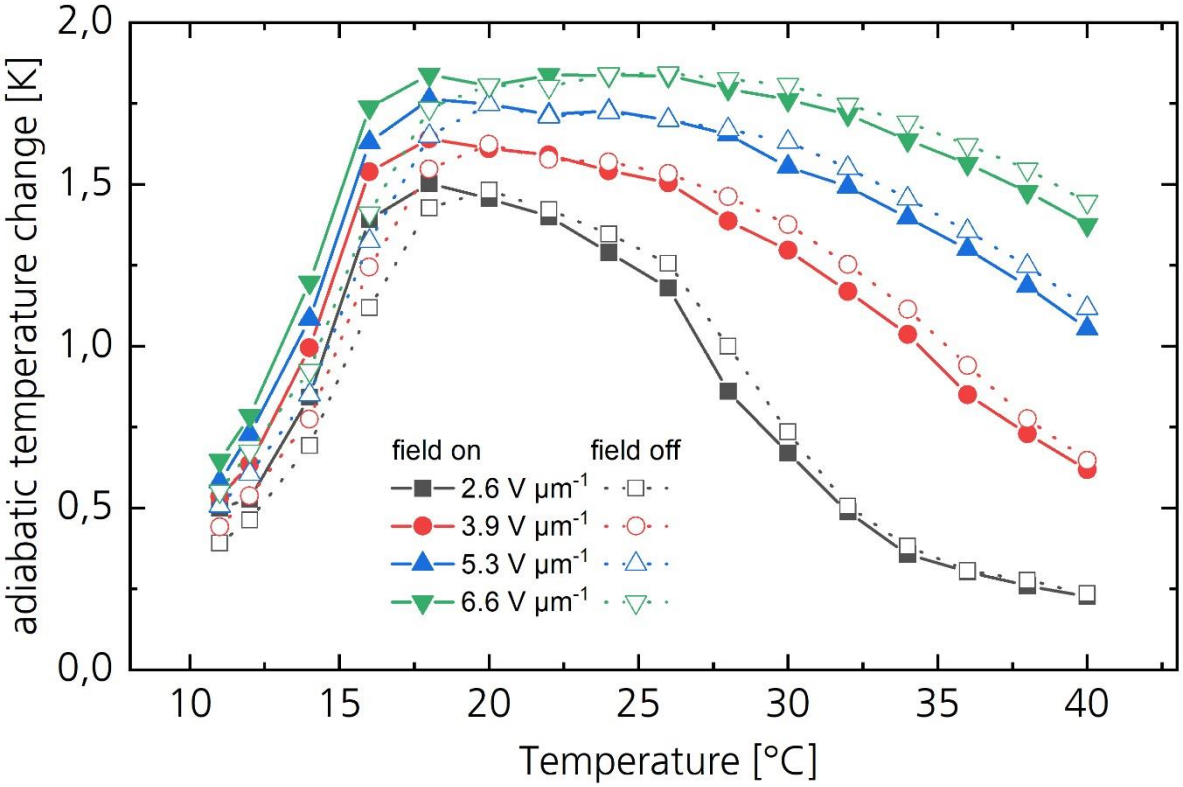

Fig. S7.

The temperature change on the surface of the components, when applying different fields was measured in air for a range of temperatures. The adiabatic temperature change was measured with a thermocouple. The temperature was set with a chiller, connected to a heat exchange plate in the same container as the PST MLC.

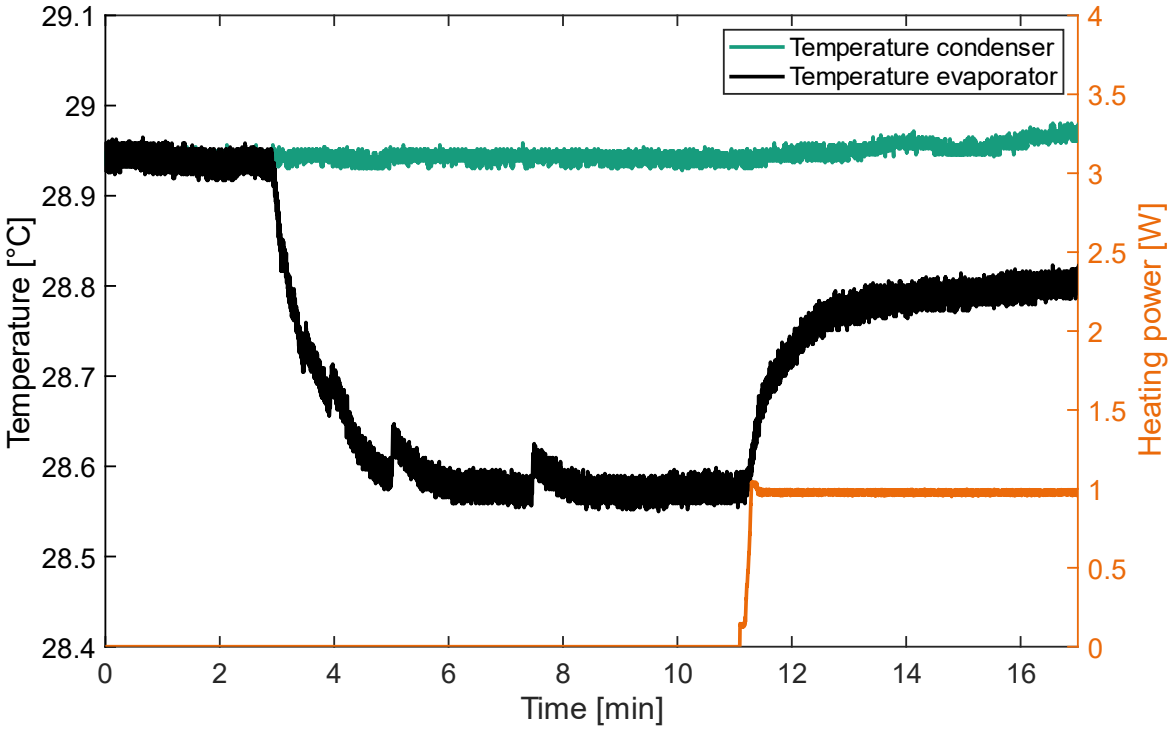

Fig. S8.

Temporal evolution of the condenser and evaporator temperatures of our system. After application of a sinusoidal voltage to the electrocaloric components a temperature difference establishes (no load condition). When the evaporator is heated, the established temperature difference reduces. For each heating power the steady state temperature difference is recorded (corresponding to one data point in fig. S9).

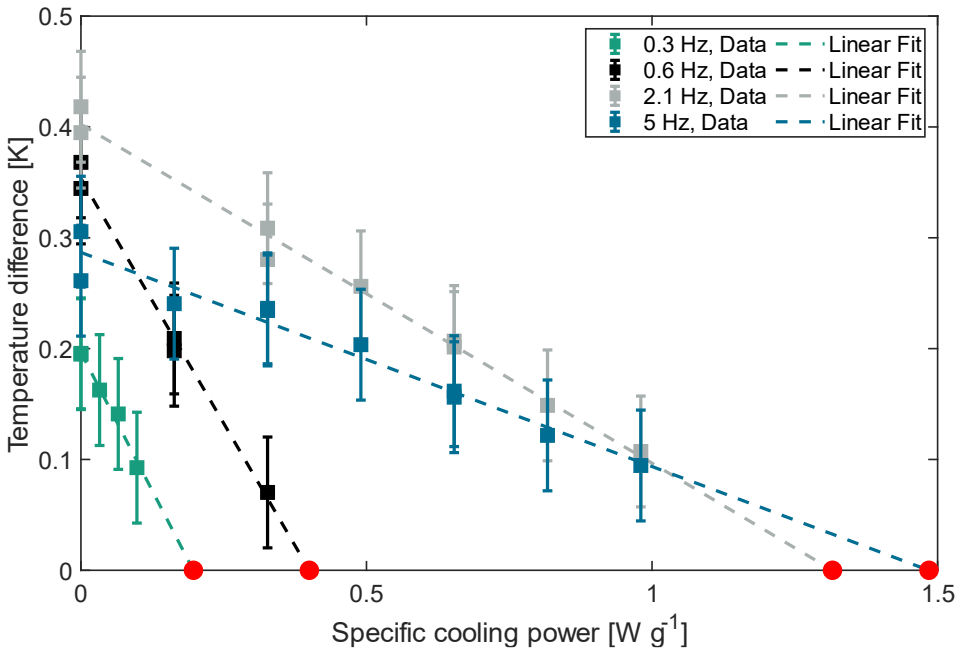

Fig. S9.

The achieved temperature span is plotted against the specific cooling power for different frequencies. The raw data is fitted with a linear regression for the different cycle frequencies. The interception of the fit with the x-axis ($\Delta T = 0$, marked with red dots) is used as the specific cooling power $\dot{q}$ for each frequency.

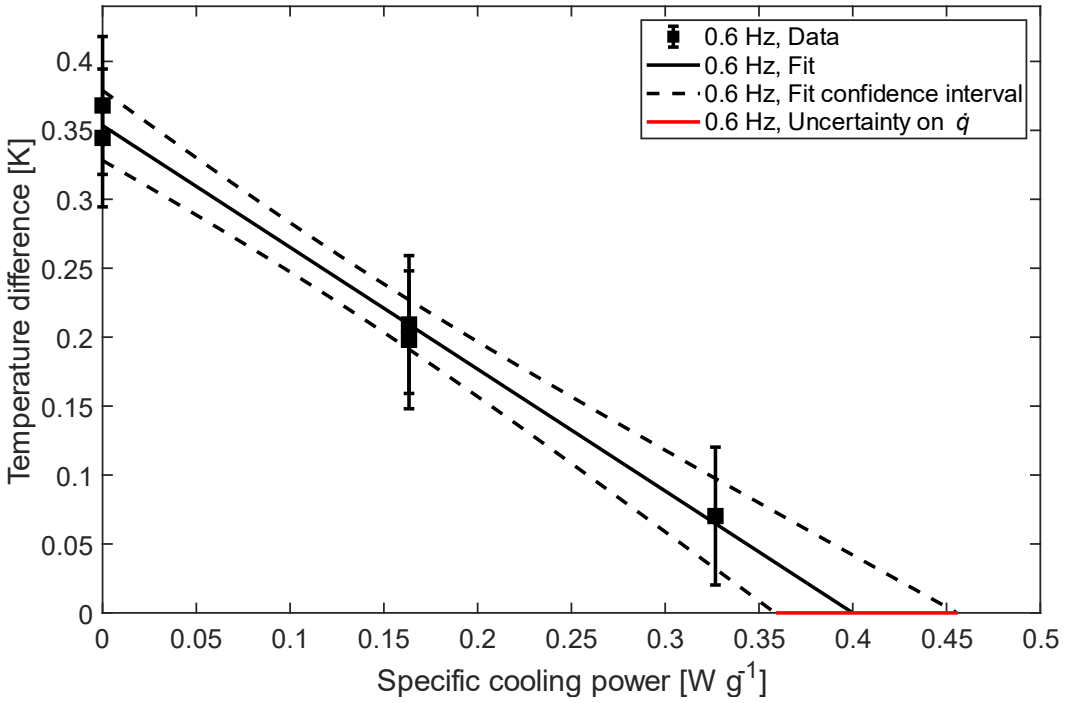

Fig. S10.

Uncertainty of specific cooling power. The uncertainty of the specific cooling power $\dot{q}(\Delta T = 0)$ is calculated from the interception of the lower and upper 95 % confidence interval of the linear regression with the x-axis ($\Delta T = 0$).

For higher frequencies the slope is lower, therefore the uncertainty is higher.

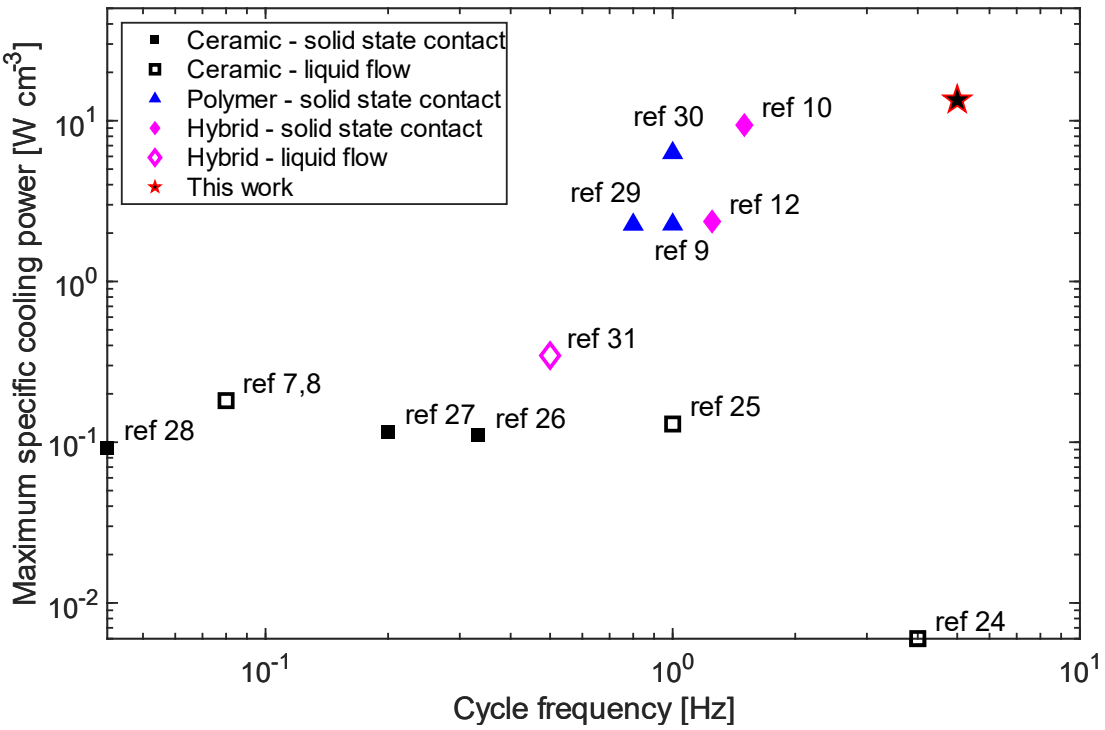

Fig. S11.

Maximum specific cooling power per active volume of electrocaloric prototype operated at their optimum cycle frequency. The empty symbols refer to all prototype, which use fluids for the heat transport, the filled symbols refer to all prototype which use solid state contact for heat transfer. This work, which uses evaporation and condensation as a heat transfer mechanism is shown as a star.

Table S1.

Comparison of cooling powers of different prototypes. Used ceramic EC-materials are $PbSc_{0.5}Ta_{0.5}O_3$ (PST), (1-*x*)$Pb(Mg_{1/3}Nb_{2/3})O_3$–*x*$PbTiO_3$ (PMN-*x*PT), $PbZr_{0.95}Ti_{0.05}O_3$ (PZT) or $BaTiO_3$ (BTO). They are either bulk material or multilayer capacitors (MLCs). Polymer EC-material is based on polyvinylidene difluoride (PVDF). Hybrid materials used $Ba_{0.6}Sr_{0.4}TiO_3$ (BST) or $Ba_xSr_{1-x}TiO_3$ (BSTO) nanoparticles (NP) or a $Ba_{0.85}Ca_{0.15}Zr_{0.1}Ti_{0.9}O_3$ (BCZT) network within PVDF.

Reference	Heat transfer mechanism	EC-material	m_{active} [g]	Frequency [Hz]	$\dot{q}$ [W g^{-1}]	$\dot{q}$ [W cm^{-3}]	$\dot{Q}$ [W]
[24]	Fluid-convection	PST-bulk	14 a)	4	0.0007	0.006	0.01
[25]	Fluid-convection	PMN-bulk	11.7	1	0.02	0.13	0.23
[7,8]	Fluid-convection	PST MLCs	11.4 b)	0,08	0.02	0.181	0.23
[26]	Solid state contact	BTO MLCs	0.87	0.33	0.041	0.111	0.036
[27]	Solid state contact	PST MLCs	6.4 c)	0.2	0.013	0.116	0.085
[28]	Solid state contact	BTO MLCs	1.09	0.04	0.015	0.092	0.017
[29]	Solid state contact	PVDF MLCs	0.105	0.8	2.83	2.260	0.30
[9]	Solid state contact	PVDF MLCs	0.7	1	1.29	2.265	0.91
[30]	Solid state contact	PVDF MLCs	0.196	1	3.6	6.300	0.34
[10]	Solid state contact	PVDF MLCs with BST NP	0.060 d)	1.5	3.95	9.390	0.24
[12]	Solid state contact	BCZT network in PVDF	0.156 e)	1.25	1.13	2.360	0.17
[31]	Fluid-convection	PVDF with BSTO NP	--	0.5	0.35	0.702 f)	--
This work	Evaporation and condensation	PST MLCs	1.53	5	1.48	13.47 g)	2.2

a) Not stated, whether it is active or total mass.
b) It was assumed that 60% of the mass were active as stated in [8].
c) Active volume was calculated by dividing absolute cooling power by volumetric cooling power. Mass was calculated by multiplying volume with density (given in the supplementary information).
d) Active volume of all 9 pixels is calculated to be 25.1 mm^3. Density is 2.38 g cm^{-3} (given in the supplementary information of the publication).
e) Active volume is 75 mm^3. Density was given by authors on request with 2.08 g cm^{-3}.
f) Almost all the volume/mass is active. This should be considered, when comparing sizes/masses of prototype.
g) Using a PST density of 9.07 g cm^{-3} [21].